Pergamon

Int. J. Heat Mass Transfer. Vol. 37, No. 17, pp. 2723–2736, 1994

0017-9310/94 $7.00+0.00

0017-9310(94)E0093-A

Heat and mass transfer in a separated flow region for high Prandtl and Schmidt numbers under pulsatile conditions

PINGPING MA, XIANMING LI† and DAVID N. KU‡

School of Mechanical Engineering, Georgia Institute of Technology, Atlanta, GA 30332-0405, U.S.A.

† Fluent Inc., 10 Cavendish Court, Lebanon, NH 03766, U.S.A.

(*Received* 3 *May* 1993 *and in final form* 28 *February* 1994)

Abstract—Heat and mass transfer phenomena were studied in the sudden expansion region of a pipe under steady and pulsatile conditions. The Prandtl number was varied from 100 to 12000 and the flow was characterized for both uniform and parabolic entrance velocity profiles. A uniform velocity profile was used for pulsatile flow. It was found that heat transfer in the recirculation region was maximal near the area where wall shear was minimal. Blunting of the inlet profile caused the point of maximum heat transfer to move upstream. There was a nonlinear effect of Prandtl number on heat transfer which plateaued for $Pr > 10^3$. The wall shear rate in the separation zone varied markedly with pulsatile flows, but the wall heat transfer remained relatively constant. The time-averaged pulsatile heat transfer at the wall was approximately the same as with steady flow with the mean Reynolds number. However, the isotherms within the pulsatile flow were markedly different from steady flow. The results demonstrate the complexity of separation flows and identify characteristic regions of high and low heat/mass transfer for high Prandtl/Schmidt pulsatile flow.

1. INTRODUCTION

TRANSPORT processes in separated pipe flows abound in nature and in industrial applications. Heat transfer in machine lubrication and compact heat exchangers can be in the laminar regime and have areas of flow separation. Devices such as combustor and chemical mixing equipment routinely employ flow separation to enhance performance. Blood flow in the human arterial system also can exhibit separated regions which may contribute to atherosclerotic plaque formation. Fluid flow and heat/mass transfer in the recirculation and reattachment regions following a sudden pipe expansion are important processes from both theoretical and practical perspectives. Much published work is available regarding the fluid dynamic aspects of flows in a sudden expansion for steady flow [1–4]. In addition, the corresponding heat transfer problem has also gained considerable attention [5–8]. However, most of the reported measurements of heat transfer have been conducted under turbulent flow conditions with moderate Prandtl number fluids. The heat/mass transfer for flows under laminar conditions are not as well documented.

Laminar sudden expansion flow is characterized by the existence of a recirculation zone located immediately downstream of the expansion step, and a reattachment point. The reattachment length, l_r, is primarily a function of the inlet Reynolds number (Re_d) and step height (s). The relationship between l_r and Re_d was found to be linear up to $Re_d < 916$ [1, 4], beyond which the reattachment length became shorter due to random fluctuations. On the other hand, the reattachment length varied nonlinearly with step height [3]. In general, the reattachment length was longer with a parabolic inlet profile than with a uniform inlet profile.

The parallel problem of laminar heat and/or mass transfer in the separation and reattachment regions has not received much attention. The literature mostly deals with turbulent flow. Ede and co-workers [5] measured the local heat transfer of water downstream of a sudden expansion with $d/D = 0.5$. The experiments were held under constant heat flux conditions for upstream Reynolds numbers from 800 to 100000 and a range of Prandtl number from about 7 to 11. The heat transfer coefficient along the expanded pipe was always greater than the corresponding fully developed pipe flow value. Furthermore, the heat transfer coefficients at $x/D < 6$ were three to four times greater than those at larger values of x/D for the entire test Reynolds number range. The pattern of heat transfer variation along the pipe was found to be independent of the Reynolds number in the range

‡Author to whom correspondence should be addressed.

NOMENCLATURE

A	amplitude of oscillation
b	source term in the discretization equation
c	specific heat
d	inlet pipe diameter
D	pipe diameter after sudden expansion
$\mathscr{D}$	species diffusion coefficient
h	heat transfer coefficient
h_m	mass transfer coefficient
k	thermal conductivity
l_r	shear layer reattachment length
L	length of expanded pipe
p	pressure
r	radial coordinate
s	step height
S	generic source term
t	time
t_p	period of oscillation
T	temperature
T_{in}	inlet fluid temperature
T_w	wall temperature
ΔT	characteristic temperature difference
u	axial velocity component
$\bar{u}$	average velocity at the inlet
U	characteristic velocity, average velocity in the expanded pipe
v	radial velocity component
x	axial coordinate
Y	species mass fraction.

Greek symbols

α	thermal diffusivity
δ	boundary-layer thickness
Γ	generic diffusion coefficient
μ	dynamic viscosity
ρ	density
ν	kinematic viscosity
τ_w	wall shear stress
ϕ	generic dependent variable
Φ	dissipation function
ω	circular frequency.

Dimensionless groups

$Br = \mu U^2/(k\Delta T)$	Brinkmann number
$C_f = \tau_w/(\rho U^2/2)$	Fanning friction coefficient
$Nu = hD/\lambda$	Nusselt number
$Pr = c\mu/k$	Prandtl number
$Re_d = \rho \bar{u} d/\mu$	Reynolds number
$Sc = \mu/(\rho\mathscr{D})$	Schmidt number
$Sh = h_m D/(\rho\mathscr{D})$	Sherwood number
$Wo = (D/2)\sqrt{\omega/\nu}$	Womersley number.

investigated, yet the magnitude of heat transfer coefficient decreased slightly as the Reynolds number increased. Prud'homme and Elghobashi [6] obtained a numerical prediction for the heat transfer coefficient of turbulent flow in a sudden pipe expansion with a constant flux wall. It was found that the Nusselt number along the expanded wall was greater than the corresponding fully developed value, and the maximum Nusselt number occurred at approximately one step height downstream of the reattachment point. However, the location of the maximum Nusselt number tended to move upstream as the Reynolds number increased. Baughn and co-workers [7] measured the heat transfer downstream of an axisymmetric sudden expansion for a uniform wall temperature boundary condition with a heat flux sensor. The nominal diameter ratio was 0.4, and the flow was fully developed at the inlet of the expansion. As the upstream Reynolds number was increased from 4300 to 44 500, the maximum Nusselt number progressively shifted upstream from 12 to 9 step heights from the expansion step, whereas the magnitude decreased from 5.6 to 3.9 times greater than the corresponding fully developed pipe flow values.

Fletcher *et al.* [8] carried out mass transfer computations for laminar steady flow in an axisymmetric sudden expansion geometry for $Re_d < 1500$ and $Sc < 1000$. The found that the results of mass transfer were sensitive to upstream velocity profile, and that the position of maximum mass transfer was always within the flow separation region. Generally, the mass transfer peak approached or even passed the reattachment point as Sc increased to about 20, and then moved upstream again as Sc increased further.

Biological flows are pulsatile because of the pumping motion of the heart. Previous research has shown that atherosclerotic plaque often occurs in areas of flow separation [9–11]. A leading hypothesis for atherogenesis is that the mass transfer of material between the vessel wall and the laminal blood is impaired in regions of flow separation [9]. In order to test this hypothesis, it is essential to understand the fluid flow and mass transfer phenomena of separation regions under pulsatile-flow conditions.

Several experimental and analytical investigations of flow and heat transfer have also been carried out for pulsatile flow through straight pipes [12–22]. However, little work has been reported on heat or mass transfer characteristics in separation regions of pulsatile flow. Flow and heat transfer in straight cylindrical pipes under pulsatile flow conditions are influenced by many parameters such as flow regime, inlet velocity profile, frequency and amplitude of oscillation, and the fluid Prandtl number. Due to the large number of control parameters and different methodologies, previous experimental studies appear to

show conflicting results on the effect of pulsation on heat transfer. For instance, it has been observed that the flow oscillations can either enhance [12–15] or reduce [16, 17] heat transfer relative to equivalent steady flows. Simultaneous augmentation and reduction have also been detected at different locations of one experimental set-up [18, 19]. Others concluded that the transfer rates increase or decrease relative to the steady-flow rate depending on values of the pulsating frequency and amplitude [20–23]. In a recent numerical study, Cho and Hyun [21] showed that the effect of pulsatility on heat transfer coefficient became prominent for fluids with low Prandtl number ($Pr < 1$). Despite the controversy on the details, one point is clear: the effect of pulsatility on heat transfer in straight pipes appears to exhibit small variations in comparison with the corresponding shear stress.

In this study, the distributions of wall shear stress and heat/mass transfer coefficient are detailed for flow through an axisymmetric sudden expansion using computational modelling. The axisymmetric sudden expansion geometry was selected because it represents a situation of permanent flow separation even with pulsatile flow. The results provide a detailed description of the fluid flow and heat/mass transfer characteristics under the combined influence of flow separation, high Prandtl number, and pulsatility.

2. METHODS

Because of difficulties in obtaining accurate mass transfer measurements with fine resolution, a numerical approach was chosen. Computational fluid dynamics (CFD) solutions have the important advantage of providing velocity and temperature data at every point within the flow field which can demonstrate the local variations of quantities such as shear stress and heat/mass transfer coefficient along the wall with much finer resolution than possible experimentally. For this study, the governing equations of fluid flow and heat transfer were discretized with the control volume formulation and solved by the SIMPLE algorithm [24, 25]. The validity of the numerical calculations was verified by grid-dependence and experimental studies for steady flow [26]. The calculation results of wall shear stress and heat transfer coefficient were compared with the corresponding values of steady flow at the same instantaneous Reynolds numbers.

2.1. *Governing equations*

The time-dependent, two-dimensional momentum and energy conservation equations were applied to an incompressible Newtonian fluid for the numerical analysis of the pulsatile flow and heat-transer phenomena in the axisymmetric pipe expansion. The physical properties were assumed to be constant. The origin of the coordinate system is at the centerline of the inlet pipe at the step, x is the axial coordinate and r is the radial coordinate (Fig. 1). The equations can be written as

mass conservation:

$$\frac{\partial u}{\partial x}+\frac{1}{r}\frac{\partial}{\partial r}(rv)=0 \tag{1}$$

momentum conservation:

$$\frac{\partial u}{\partial t}+u\frac{\partial u}{\partial x}+v\frac{\partial u}{\partial r}=-\frac{1}{\rho}\frac{\partial p}{\partial x}+\nu\left[\frac{\partial^2 u}{\partial x^2}+\frac{1}{r}\frac{\partial}{\partial r}\left(r\frac{\partial u}{\partial r}\right)\right] \tag{2}$$

$$\frac{\partial v}{\partial t}+u\frac{\partial v}{\partial x}+v\frac{\partial v}{\partial r}=-\frac{1}{\rho}\frac{\partial p}{\partial r}+\nu\left[\frac{\partial^2 v}{\partial x^2}+\frac{1}{r}\frac{\partial}{\partial r}\left(r\frac{\partial v}{\partial r}\right)-\frac{v}{r^2}\right] \tag{3}$$

energy conservation:

$$\frac{\partial T}{\partial t}+u\frac{\partial T}{\partial x}+v\frac{\partial T}{\partial r}=\frac{k}{\rho c}\left[\frac{\partial^2 T}{\partial x^2}+\frac{1}{r}\frac{\partial}{\partial r}\left(r\frac{\partial T}{\partial r}\right)\right]+\frac{\mu}{\rho c}\Phi \tag{4}$$

where u is the axial velocity component, v the radial velocity component, T the fluid temperature, ν the kinematic viscosity, k the thermal conductivity, ρ the fluid density, and c the specific heat.

The dissipation function Φ is

$$\Phi=2\left[\left(\frac{\partial u}{\partial x}\right)^2+\left(\frac{\partial v}{\partial r}\right)^2+\left(\frac{v}{r}\right)^2\right]+\left(\frac{\partial u}{\partial r}+\frac{\partial v}{\partial x}\right)^2. \tag{5}$$

The mass conservation equation for an inert species is

$$\frac{\partial Y}{\partial t}+u\frac{\partial Y}{\partial x}+v\frac{\partial Y}{\partial r}=\mathscr{D}\left[\frac{\partial^2 Y}{\partial x^2}+\frac{1}{r}\frac{\partial}{\partial r}\left(r\frac{\partial Y}{\partial r}\right)\right]. \tag{6}$$

A comparison of the energy equation (4) with the mass transfer equation (6) reveals that the temperature and the species mass fraction are similar if the viscous dissipation effect Φ is negligible, and the mass diffusivity and the thermal diffusivity are equal: $\mathscr{D}=\alpha$. The latter condition is also equivalent to $Pr=Sc$.

The importance of the last term in the energy equation (4) is characterized by the Brinkmann number

$$Br=\frac{\mu U^2}{k(\Delta T)} \tag{7}$$

where U is the characteristic velocity in the flow and ΔT is a characteristic temperature difference. This dimensionless parameter can be interpreted as the ratio of viscous heat generation to heat loss by conduction. When Br is of the order of unity or greater, the viscous dissipation effect becomes significant. This

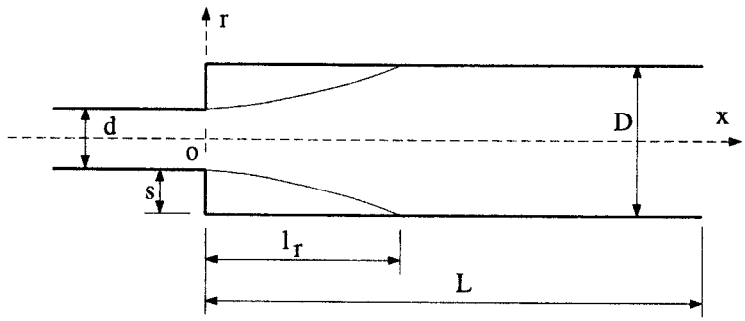

FIG. 1. Schematic diagram of the sudden expansion with depiction of the coordinate system.

situation occurs when the Prandtl number of the fluid is large, such as considered in the present study.

Heat transfer results are directly applicable for mass transfer predictions provided that Sc is substituted for Pr in the absence of viscous heating. This observation enables us to extend the heat-transfer results to mass transfer wherever appropriate.

2.2. *Boundary conditions*

For steady flows, both uniform and parabolic inlet velocity profiles are used. The fluid is maintained at a constant temperature which is higher than that of the walls. The walls are treated as no-slip with a constant temperature. For steady flow at the inlet,

$$\text{uniform:} \quad u = \frac{v}{d} Re_d \tag{8}$$

$$\text{parabolic:} \quad u = \frac{2v}{d} Re_d \left(1 - \frac{4r^2}{d^2}\right) \tag{9}$$

$$T = T_{in}. \tag{10}$$

For pulsatile flow, the fluid velocity profile in a straight pipe is a complicated function of time and radial position [27]. For simplicity, the axial velocity component in this study is assumed to be spatially uniform, but sinusoidal in time:

$$u = v \frac{\overline{Re_d}}{d} \left[1 + A \sin\left(\frac{2\pi}{t_p} t\right)\right] \tag{11}$$

where $\overline{Re_d}$ is the mean entrance Reynolds number, A is the amplitude of oscillation, and t_p is the period. Initially, for $t = 0^-$, $u = 0$, $v = 0$, $T = T_w$ at all locations. Then, for $t = 0^+$, the conditions are

$$\text{inlet:} \quad v = 0 \quad T = T_{in} \tag{12}$$

$$\text{walls:} \quad u = 0 \quad v = 0 \quad T = T_w. \tag{13}$$

A long domain of approximately $66D$ was chosen to minimize the boundary influence of the downstream conditions. At the outlet, all variables are assumed to be fully developed with a zero-axial gradient condition:

$$\text{outlet:} \quad \frac{\partial u}{\partial x} = 0 \quad \frac{\partial v}{\partial x} = 0 \quad \frac{\partial T}{\partial x} = 0. \tag{14}$$

Across a symmetric boundary, all normal gradients are zero in addition to zero cross flow:

axis of symmetry:

$$v = 0 \quad \frac{\partial u}{\partial r} = 0 \quad \frac{\partial v}{\partial r} = 0 \quad \frac{\partial T}{\partial r} = 0. \tag{15}$$

2.3. *Physical parameters*

All numerical values of the computational model parameters are listed in Table 1. In the presentation of the results, two additional dimensionless parameters were involved. The wall shear stress, and heat and mass transfer coefficients were presented in terms of friction coefficient, local Nusselt number and Sherwood number, respectively:

$$C_f = \frac{\tau_w}{\rho U^2/2} \quad Nu = \frac{hD}{k} \quad Sh = \frac{h_m D}{\rho \mathscr{D}}. \tag{16}$$

Furthermore, these quantities were normalized by values at their respective fully developed states to facilitate comparison among different flow conditions:

$$C_{f,fd} = 16/Re_D \quad Nu_{fd} = 3.658 \quad Sh_{fd} = 3.658 \tag{17}$$

where Re_D is the Reynolds number based on the average velocity U and diameter D after the expansion, and $C_{f,fd}$ and Nu_{fd} correspond to the fully developed pipe flow values after the expansion far downstream subject to a constant surface temperature. Note that the corresponding mass transfer quantities are also listed.

The pulsatility for the relevant hemodynamic problem corresponds to a Womersley number of 4.1, defined as $Wo = D/2\sqrt{\omega/v}$, where ω is the circular frequency: $\omega = 2\pi/t_p$.

2.4. *Numerical procedures*

The governing partial differential equations (1)–(4) may be recast into the following form:

$$\frac{\partial}{\partial t}(\rho\phi) + \frac{\partial}{\partial x_i}(\rho u_i \phi) = \frac{\partial}{\partial x_i}\left(\Gamma \frac{\partial \phi}{\partial x_i}\right) + S \tag{18}$$

where the generic dependent variable ϕ, diffusion coefficient Γ, and source term S are listed in Table 2.

Table 1. Parameters used in the numerical analysis

Symbol	Description	Unit	Standard case	High-Pr Case 1	High-Pr Case 2
	Material	—	Silicone DC200-10cS (298 K)	Glycerin (313 K)	Glycerin (293 K)
d	Inlet pipe diameter	mm	14.5	14.5	14.5
D	Downstream diameter	mm	30.5	30.5	30.5
s	Step height	mm	8.0	8.0	8.0
L	Length of domain	m	2.0	2.0	2.0
T_{in}	Inlet fluid temperature	K	303	303	303
T_w	Wall temperature	K	298	298	298
ρ	Density	kg m^{-3}	935	1249	1261
μ	Dynamic viscosity	Pa s	9.35×10^{-3}	0.2835	1.4123
k	Thermal conductivity	W m^{-1} s^{-1}	0.134	0.285	0.285
c	Specific heat	J kg^{-1} K^{-1}	1506.2	2460	2350
Re_d	Inlet Reynolds number	—	0–950	500	500
Pr	Prandtl number	—	105	2500	12 000
Br	Brinkmann number	—	8.47×10^{-5}	0.623	75.5

A discretized version of this equation is derived by integrating it over a control volume with surface fluxes evaluated by a quadratic upwind interpolation method [25]. The time-dependent term is treated with a fully-implicit approach. Applying this integration procedure to all control volumes in the field results in a set of algebraic equations which forms a band matrix. Similar procedures may be applied to all dependent variables to generate the algebraic equation system. This algebraic equation system is solved in a special procedure implemented in a commercially available CFD package [24].

A major difficulty in studying high-Pr heat transfer is the fine grid spacing near the wall required to capture the temperature gradients correctly. Non-uniform grids of 417×26 for the pulsatile flow and 480×36 for the steady flows were employed with high resolution near the wall and in the recirculation region. A grid dependence study showed that the maximum errors for wall shear stress and heat transfer coefficient were 1% and 5%, respectively. The convergence tolerance was set at 10^{-3} for flow variables and 10^{-6} for enthalpy. For pulsatile flows, the solution was assumed to be at an approximately periodic state when the heat transfer and shear stress at the wall 70 step heights downstream of the expansion varied less than 4% from cycle to cycle. Typically, the flow field reached such a periodic state in the third cycle. However, it took 19 cycles for the heat transfer to reach the same condition, because the thermal diffusivity (α) of the fluid is 105 times smaller than its diffusivity of momentum (ν).

Table 2. Identification of ϕ, Γ and S

Conservation of	ϕ	Γ	S
Mass	ρ	0	0
Axial momentum	u	μ	$-\partial p/\partial x$
Radial momentum	v	μ	$-\partial p/\partial r$
Energy (heat transfer)	T	k/c	$\mu/(\rho c)\Phi$
Species (mass transfer)	Y	$\rho\mathscr{D}$	0

The base case physical constants are for a commercially available, non-toxic silicone fluid (Dow Corning 200 fluid, 10cS) [28]. In the relevant temperature range between 298 K and 303 K, all properties of the silicone fluid varied less than 5% and can be treated as constants. The Brinkmann number was evaluated based on the average velocity in the larger pipe and the temperature difference between the inlet and the wall.

3. RESULTS

A standard case was developed to illustrate the flow and heat/mass transfer conditions in a sudden expansion region with $Re_d = 500$ and $Pr = 105$. The streamlines and isotherms in Fig. 2(a) are shown for the first 0.75 m after the step and are scaled up 10.7 times in the cross-stream direction. For a fully developed, parabolic inlet velocity profile, the recirculating flow carries hot core fluid to the wall in the separation zone. Consequently, the contours of high temperature are clustered at the wall in the recirculation zone as shown in Fig. 2. Further downstream, the temperature gradient is less steep at the wall and diffusional transport is dominant. At the exit, velocity is fully developed but the thermal entry length is approximately two orders of magnitude larger for this fluid with $Pr = 105$. Heat transfer at the wall is maximal in the recirculation zone, in contrast with wall shear which is minimal in this region. The axial position of maximum heat transfer is downstream of the minimum wall shear, closer to the reattachment point.

With different inlet velocity profiles, the location and magnitude of maximum wall heat transfer changes. The local heat transfer coefficient in the recirculation region for uniform inlet profiles is always

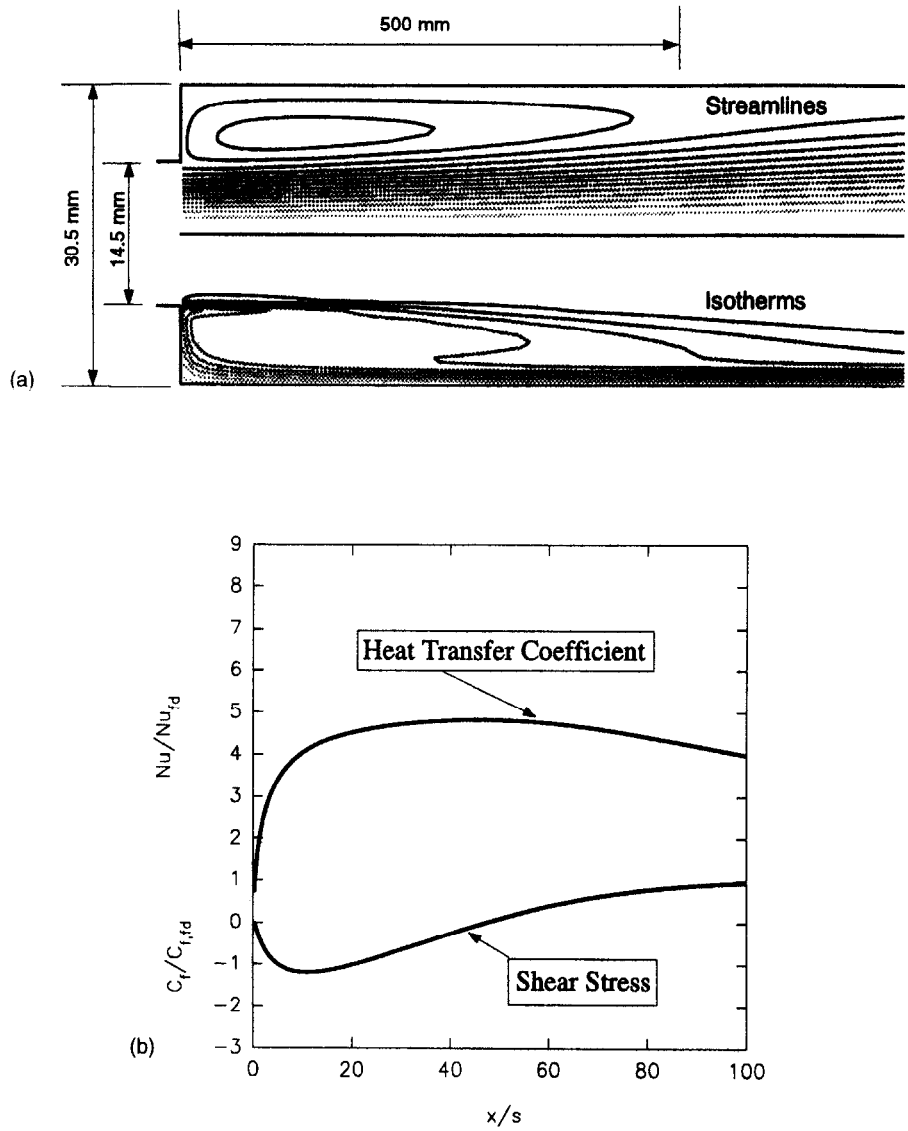

FIG. 2. Streamlines (top half, (a)), isotherms (bottom half, (a)) and wall shear stress and heat transfer coefficient distributions (b) for a steady flow of $Re_d = 500$ and $Pr = 105$ after the sudden expansion with a parabolic entrance profile.

higher than that of the fully developed pipe flow. For uniform inlet velocity profiles, the maximum heat transfer increases by almost a factor of 2. All positions move upstream and the point of maximum heat transfer moves closer to the point of minimum shear, illustrated in Fig. 3. For the same Reynolds number, a uniform inlet velocity profile gives rise to a shorter recirculation zone, a smaller minimum shear stress value, and a peak wall heat transfer coefficient 80% higher than the parabolic inlet case.

The axial locations of minimum and zero shear stresses, as well as the maximum heat transfer coefficient are displayed in Fig. 4 as functions of a range of inlet Reynolds numbers from 10 to 700. This figure indicates that reattachment length is a linear function of Reynolds number up to at least 700. Independent of inlet velocity profiles, the locations of reattachment ($\tau_w = 0$), maximum heat transfer ($h = h_{max}$) and minimum shear stress (or maximum reverse shear stress, $\tau = \tau_{min}$) move downstream at constant rates with increasing Reynolds number. Uniform inlet velocity profiles give rise to shorter distances for equivalent Reynolds numbers. For flows with uniform inlet velocity profiles, the locations of maximum heat transfer are closer to those of minimum shear stress; while for flows with parabolic inlet velocity profiles, the location of maximum heat transfer are just next to the reattachment points.

As a check, the reattachment lengths predicted by the CFD code were compared with experimental measurements made by ourselves, as well as measurements made by Macagno and Hung [1] and Latornell and Pollard [4]. The present computations for a geometric expansion of $d/D = 0.475$ yielded a slope of

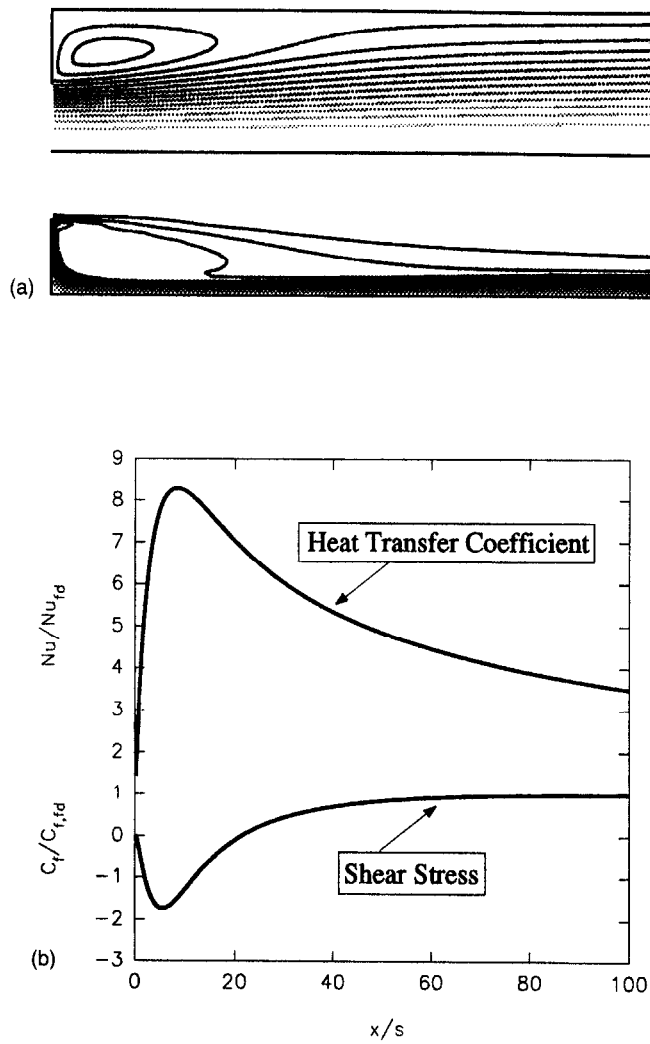

FIG. 3. Streamlines (top half, (a)), isotherms (bottom half, (a)) and wall shear stress and heat transfer coefficient distributions (b) for a steady flow of $Re_d = 500$ and $Pr = 105$ after the sudden expansion with a uniform entrance profile.

0.094 between reattachment length and Reynolds number. This slope was compared to our experimental measurements of a sudden expansion of $d/D = 0.475$ [26]. The linear relationship of reattachment length to Reynolds number was confirmed with a correlation coefficient of $r = 0.99$ and less than 3% difference in slope. For $Re_d \leqslant 300$, the experimental and computational studies of Macagno and Hung provided a linear relationship for a slope of 0.090 for $d/D = 0.500$. For $Re_d \leqslant 916$, the experimental data of Latornell and Pollard provided a slope of 0.096 with $d/D = 0.495$. Thus, the CFD solutions appear reasonable for this separated flow situation.

Prandtl number variations. As Prandtl number increases, the isotherms become more like the streamlines in shape. These contours are presented in Fig. 5 for $Pr = 2500$ and $Pr = 12\,000$. These results are given for a constant Reynolds number of 500 and clearly illustrate that wall heat transfer and wall shear are independent quantities for separated flows. The location of maximum wall heat transfer varies quite a bit over this range of Prandtl number. For low $Pr \sim 1$ and higher $Pr > 10^2$, the maximum heat transfer is located within the recirculation zone, as depicted in Fig. 6. However, for an intermediate range of $Pr \sim 10$, the maximum heat transfer occurs downstream of the reattachment point.

There exists a strong analogy between heat transfer and mass transfer. The major difference between the scalar conservation equations of species and energy lies in the viscous dissipation term of the energy equation. For fluids with Prandtl numbers below 10^3, the flow conditions in this study result in $Br \ll 1$. Thus, the last term in the energy equation (4) is negligible and low Schmidt number solutions are equivalent. However, for flows with Prandtl number greater than 10^3, the two solutions are not the same. Figure 7 illustrates the scaled wall heat transfer coefficient with

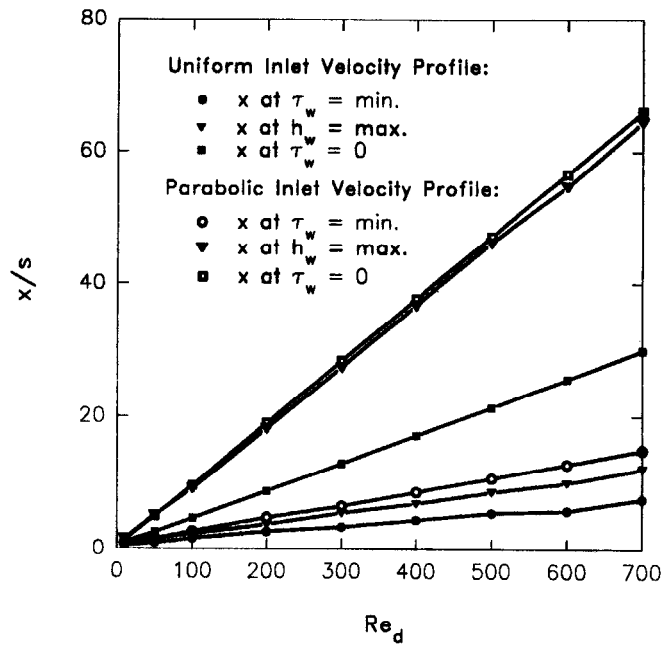

FIG. 4. Steady-flow relationships among characteristic locations of minimum shear stress (τ_w = min), maximum heat transfer coefficient (h_w = max) and reattachment point (τ_w = 0) versus Reynolds number for fluid with Pr = 105.

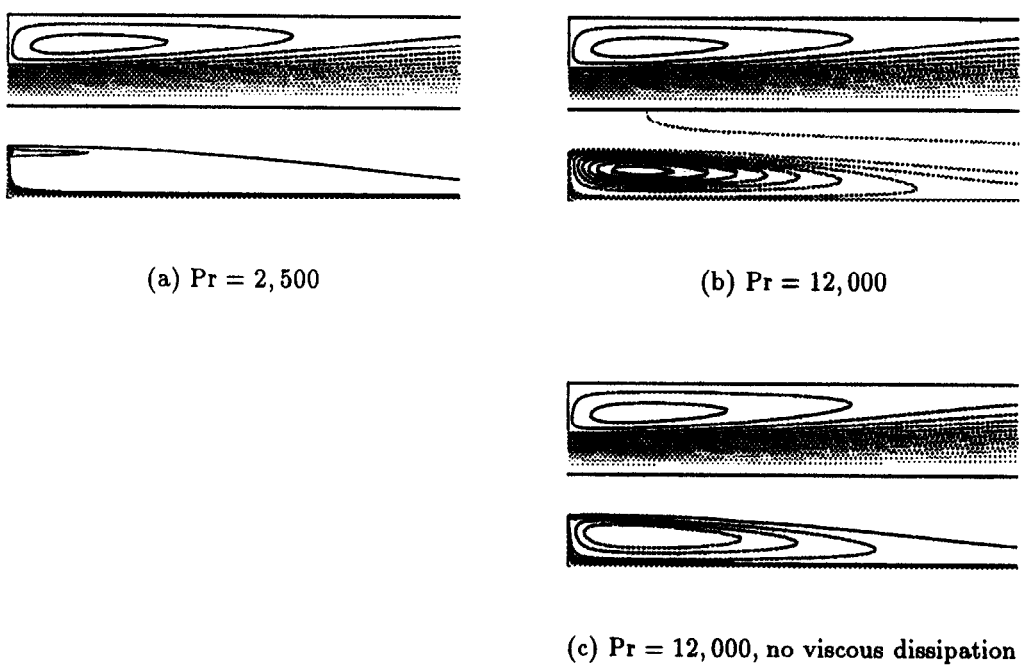

FIG. 5. Streamlines (top halves) and isotherms (bottom halves) of high-Pr steady flow at Re_d = 500.

and without the viscous dissipation term. The curves indicate that for Pr = 2500, the two conditions are essentially equivalent. However, for fluid with a Pr = 12000, the viscous dissipation generates heat, substantially raising the local temperature in the recirculation zone. This additional heat source causes an augmented heat transfer at the wall as the Brinkmann number reaches 75. Thus, a direct heat and mass transfer analogy would be appropriate for separated flows up to Pr or Sc numbers of at least 2500.

Pulsatile flow and mass transfer. The Pr for the pulsatile flow case is 105. Based on the discussion in

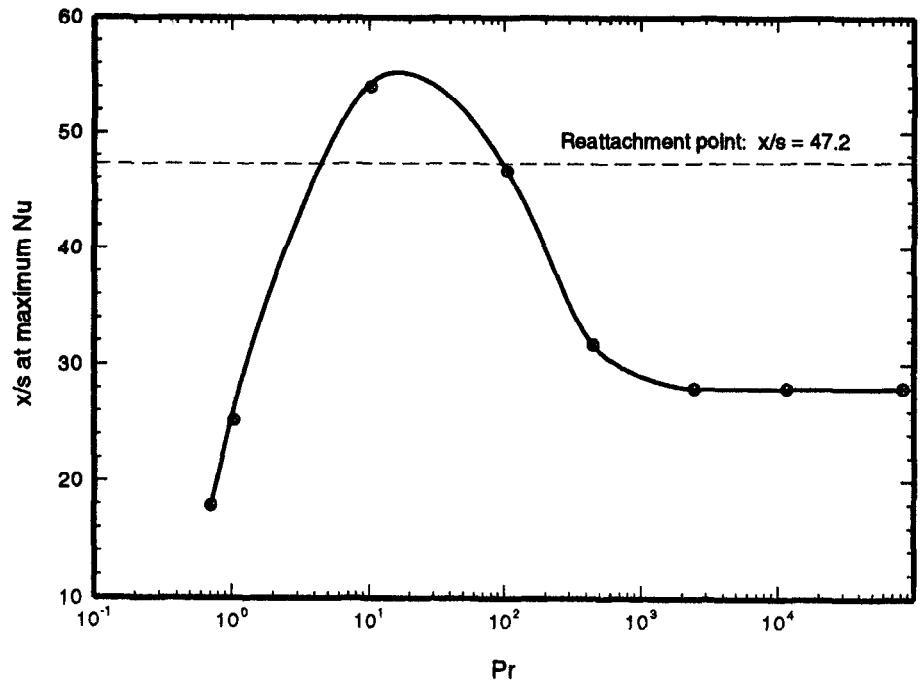

FIG. 6. Effect of Prandtl number on location of maximum heat transfer for steady flow at $Re_d = 500$ and a parabolic inlet velocity profile.

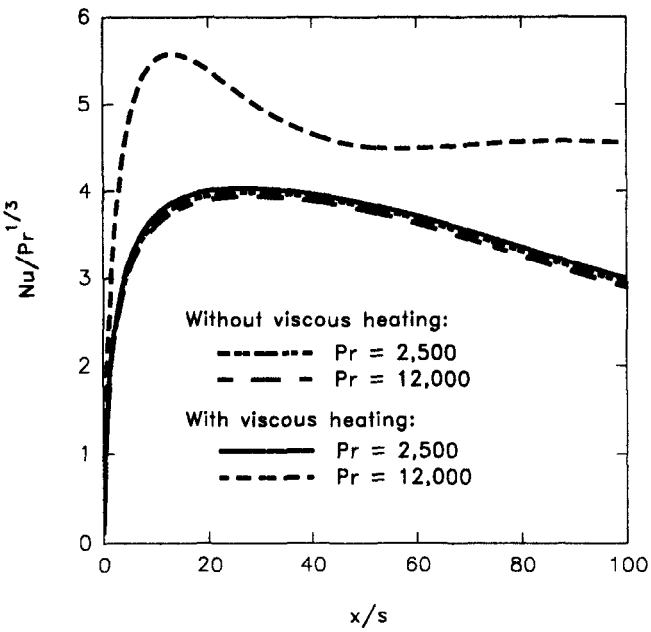

FIG. 7. Effect of viscous heating on the applicability of the heat and mass transfer analogy in the sudden expansion region. The mass transfer curves are identical to those of heat transfer without viscous heating. When scaled by $Pr^{1/3}$ or $Sc^{1/3}$, the mass transfer and heat transfer relations reduce to a single curve if the viscous heating effect in heat transfer is negligible.

the preceding section, heat transfer and mass transfer are equivalent. We shall use these terms interchangeably in the discussion of pulsatile flow results. The time-dependent recirculation regions and concentration distributions at time increments of one-fifth of the oscillation period are shown in Fig. 8, when both the flow and mass transfer have reached a periodic steady state after 19 cycles. The instantaneous streamlines show considerable variation through the pulsatile cycle. At the onset of the cycle ($t/t_p = 0$), the

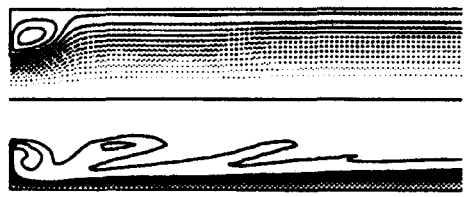

(a) $t/t_p = 0.2$

(b) $t/t_p = 0.4$

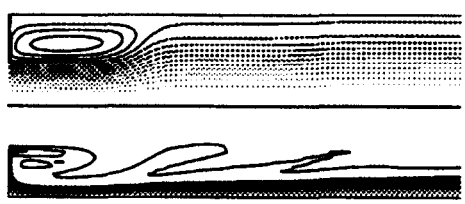

(c) $t/t_p = 0.6$

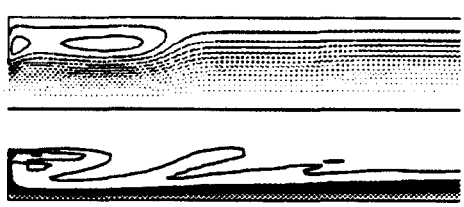

(d) $t/t_p = 0.8$

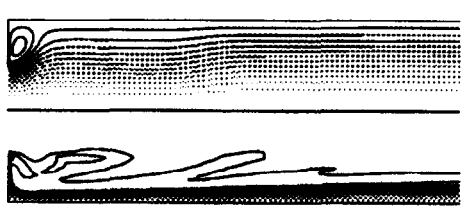

(e) $t/t_p = 1.0$

FIG. 8. Streamlines (top halves) and isoconcentration contours (bottom halves) for pulsatile flow during the nineteenth cycle with $Sc = 105$, typical of an O_2 molecule in saline ($Re_d = 300$–700). Note the dynamic behavior of the streamlines in contrast to the relatively stationary isoconcentration contours.

streamline pattern indicates that the recirculation zone is one-third the size of steady flow at the same instantaneous Re_d. The recirculation zone increases with time from the beginning of the cycle until $t/t_p = 0.8$ when a second eddy is formed and the first eddy disappears. In contrast, the isoconcentration contours change less. Even in pulsatile flow, the isoconcentration lines are clustered in the vicinity of the wall in the recirculation and reattachment regions where higher concentrations prevail. Nonetheless, the isocontours for pulsatile flow are distinctly different in shape from those for steady flow (compare Figs. 3 and 8).

Mass transfer is greatest in the recirculation region for most of the cycle. The normalized shear stress and mass transfer coefficient variations along the wall are displayed in Fig. 9 at four time instants of the nineteenth cycle, where $C_{f,fd}$ is evaluated at the mean Reynolds number. The instantaneous wall shear-stress distribution varies markedly with time, and doubles in magnitude in both the forward and reverse directions at the peak flow. In contrast, the mass transfer coefficient distribution varies by less than 8% over the pulsatile cycle and was only 9% greater in magnitude in comparison with steady flows at the mean Reynolds number.

The relationships among the locations of minimum and zero shear stresses, and maximum mass transfer coefficient during the pulsatile cycle are given in Fig. 10. The flow parameters of the minimum shear stress position and reattachment point move widely over the cycle, whereas the maximum mass transfer coefficient location shifts only slightly within a narrow range. The maximum mass transfer locations are close to the regions of maximum reverse shear stress. However, the maximum mass transfer positions do not always remain in between the locations of zero-shear and minimum-shear, as observed with steady flows. In general, the maximum mass transfer at the wall during pulsatile flow is located close to the point seen with steady flows at the mean Reynolds number (66 mm downstream of the step versus 69 mm for steady flow at $Re_d = 500$, $l_r = 376$ mm, Fig. 4).

4. DISCUSSION

Heat/mass transfer and fluid flow analyses were carried out for the axisymmetric sudden expansion configuration as an example of permanently separated flows. The separation region involved complex secondary flow patterns and interactions between energy/species and momentum transport. For a sudden expansion with separated flows, heat/mass diffused from the core flow and then convected directly to the wall by the recirculatory flow. This convection yielded heat/mass transfer coefficients in the recirculating region up to nine times higher than the corresponding value for fully developed laminar flow in a pipe of the same diameter. The locations of reattachment point, minimum shear stress and maximum heat/mass trans-

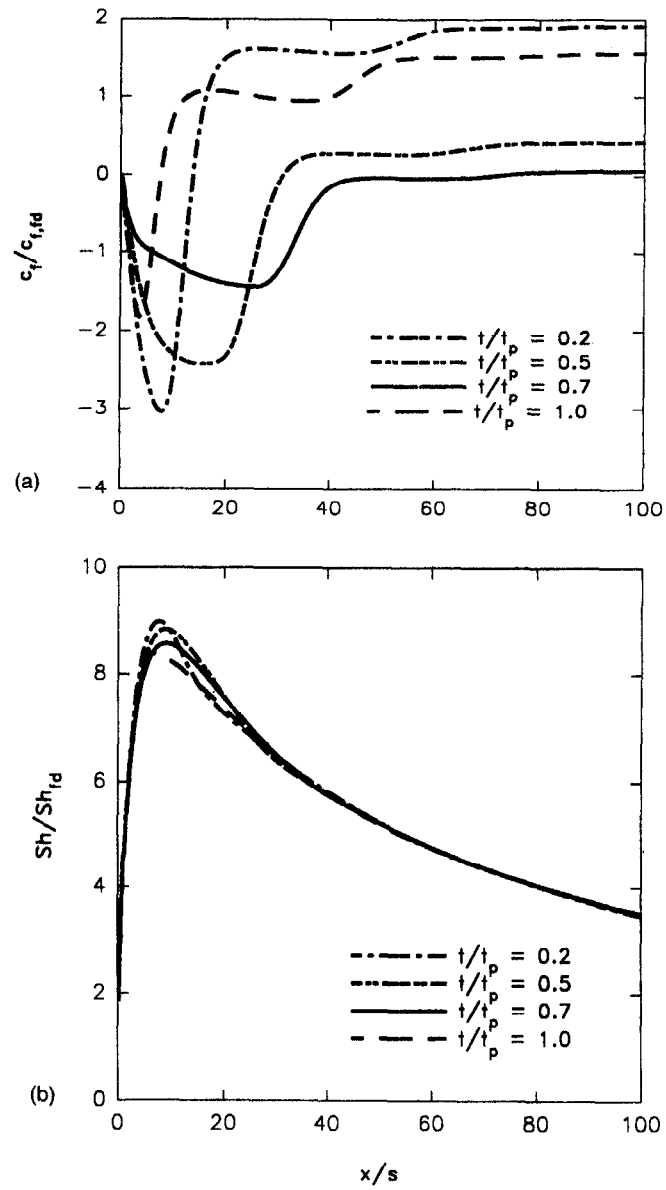

FIG. 9. Wall shear stress at four selected time points for a sinusoidally-varying pulsatile flow (a). Wall mass transfer coefficient distribution for the pulsatile flow at four selected time points (b). Note the relative constancy of mass transfer.

fer varied linearly with inlet Reynolds numbers in steady flows, whereas, for pulsatile flows, the maximum heat/mass transfer location was almost invariant with respect to the instantaneous flow. The pulsatile heat and mass transfer was similar in magnitude to that found for the equivalent time-averaged steady flows.

The maximum heat/mass transfer coefficient for a uniform inlet velocity profile was approximately 80% higher than that of a parabolic profile case. Throughout the recirculation region, a uniform inlet velocity shape produced a heat/mass transfer coefficient approximately 50% higher than parabolic inlet conditions, because the blunt entrance velocity profile gave rise to a larger vorticity magnitude at the expansion step and a stronger recirculation. In the light of the inclined jet impingement configuration, the edge of the core flow reaches the pipe wall earlier and with higher momentum which results in a higher heat/mass transfer coefficient for a uniform inlet velocity profile.

Usually, in flows with $Pr > 10$, the diffusional transport mechanism may be considered weak. In the presence of secondary flow, however, this may be incorrect as indicated in the standard case with $Pr = 105$. Heat transfer occurs between the core and the separated flow by diffusion, even in the presence of a dividing streamline. The diffused heat is then convected by the recirculating current to the wall in the separation zone, causing a steep thermal gradient at this point [29]. The mechanism of heat transfer augmentation in the

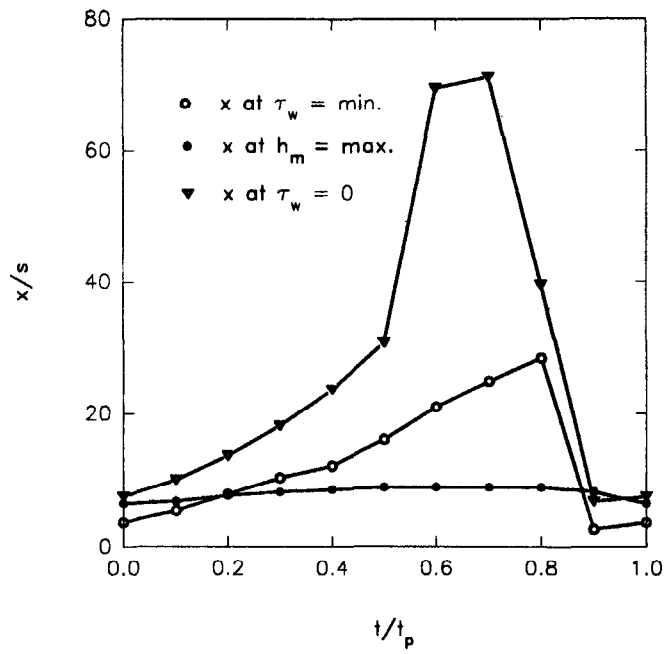

FIG. 10. Relationship among characteristic locations of minimum shear stress (τ_w = min), maximum mass transfer coefficient (h_m = max) and reattachment point (τ_w = 0) for the pulsatile flow.

separated region is analogous to heat transfer behavior in the inclined jet impingement configuration. Studies conducted analytically by Garg and Jayaraj [30] and experimentally by Goldstein and Franchett [31], and Sparrow and Lovell [32] show that the maximum heat transfer point is located towards the side where the jet and the surface make an acute angle. Furthermore, the smaller the angle, the greater the offset. The implication is that the maximum heat transfer location in the current study should be within the recirculation region, for the reattachment point is analogous to the geometric center. In addition, the offset increases with Reynolds number, because a larger Reynolds number gives rise to a larger reattachment length and a smaller grazing angle. These variational patterns were observed in the present study for low and high *Pr*, but not for intermediate $Pr \sim 10$. This special behavior of the reattachment point at intermediate Prandtl numbers was also observed by Fletcher *et al.* [8].

The location of maximum heat/mass transfer shifted upstream from the reattachment point towards the step with high Prandtl/Schmidt numbers (Fig. 6). This result is similar to the findings of Fletcher *et al.* [8] for a slightly lower range of Schmidt and Reynolds numbers. A further comment has to do with the viscous dissipation effect at high Prandtl numbers. The heat generation due to movements of highly viscous fluids is a unique heat source term in the transport equation of energy for high Prandtl flows yielding divergent results between heat and mass transfer for *Pr* or $Sc > 10^3$.

For straight circular pipes, Cho and Hyun [21], and Al-Haddad and Al-Binally [22] concluded that the pulsation effect on the average Nusselt number was less than 10% for *Pr* up to 10, moderate Womersley numbers, and moderate oscillation amplitudes. Similarly, McMichael and Hellum's analysis of mass transfer in straight tube pulsatile flows with *Sc* up to 10^3 found only weak effects [23]. For straight tube flow only a 10% difference in skin friction coefficient due to pulsatility was reported [21]. The pulsatile flow in a sudden expansion exhibits an instantaneous wall shear stress distribution which varied markedly with time and doubled at the peak flow in both the forward and reverse directions. In marked contrast, the instantaneous wall heat/mass transfer coefficient distribution varied only 8% with time within the recirculation region for pulsatile flow.

It is clear that the streamlines and isoconcentration contours shown in Fig. 8 are quite different. In general, the closed streamline shapes expand and contract during the cycle, leading to a shed vortex as seen in Fig. 8(d). The isoconcentration 'fingerlets' convect along with these shed vortices in a relatively uniform flow field. In our case, we observed fingerlets of mass concentration. This phenomenon may be analogous to the phenomenon of vortex-induced energy separation in which the total temperature can change in space and time creating some regions with more energy than others [33].

A limitation of this analysis for pulsatile flow is that the entrance profile was constant throughout the cycle. Blood flow near the aortic valve will typically have a blunt profile throughout the cycle as there is little entrance length for development and the

Womersley number is high [34]. For more distal arteries such as the carotid and femoral arteries, a complex Womersley-type inlet profile would be more realistic. Unfortunately, this complex inlet profile could not be readily incorporated in the existing CFD program. Nonetheless, the distinctions between the blunt and a more developed inlet profile illustrated in this study remain important to the biological problem.

In this study, the flow and heat/mass transfer characteristics in the sudden expansion model are reported in detail for three different Prandtl/Schmidt number flows with similar thermal/species diffusivities. The Prandtl number used for the pulsatile calculation was much smaller than the typical Schmidt number (10^5) used for lipoproteins mass transfer between blood and arterial walls. Higher Schmidt numbers modelling lower molecular diffusivities may need to be studied in the future. Further research into mass transfer in areas of actual arterial geometry under typical physiological flow conditions would be important to the understanding of vascular diseases.

Understanding of heat/mass transfer in separated regions has important implications to practical flows. Heat/mass transfer and fluid flow were examined in the recirculation region behind a sudden axisymmetric expansion as functions of pulsatile flow, fluid Prandtl/Schmidt number, and shape of the inlet velocity profile. The pulsatility of the flow did not appear to impact the heat/mass transfer in separate regions as strongly as the wall shear stress. There was a nonlinear effect of Prandtl/Schmidt number on heat/mass transfer which appears to plateau at approximately Pr or $Sc > 10^3$, suggesting that moderate Schmidt number modelling may be sufficient for larger proteins.

5. CONCLUSION

The laminar heat and mass transfer phenomena were studied in the sudden expansion region of a pipe under steady and pulsatile conditions. The Prandtl number was varied from 100 to 12000 and the flow was characterized for two entrance velocity profiles for steady flow: a uniform velocity and a parabola typical of fully developed flow. A uniform velocity profile was used for pulsatile flow. It was found that heat transfer in the recirculation region was maximal near the area where wall shear was minimal. Blunting of the inlet profile caused the point of maximum heat transfer to move upstream. There was a nonlinear effect of Prandtl number on heat transfer which plateaued for $Pr > 10^3$. The wall shear rate in the separation zone varied markedly with pulsatile flows, but the wall heat transfer remained relatively constant. Under the flow conditions studied in this paper, heat and mass transfer were analogous to each other until $Pr > 10^3$, beyond which the viscous heating effect became significant and the analogy broke down. The time-averged pulsatile heat transfer at the wall was approximately the same as with steady flow with the mean Reynolds number. However, the isotherms within the pulsatile flow were markedly different from steady flow. The results demonstrate the complexity of separation flows and identify characteristic regions of high and low heat/mass transfer for high Prandtl/Schmidt pulsatile flow.

Acknowledgement—This research was supported in part by NIH R29HL39437.

REFERENCES

1. E. O. Macagno and T. K. Hung, Computational and experimental study of a captive annular eddy, *J. Fluid Mech.* **28**, 43–64 (1967).
2. L. H. Back and E. J. Roschke, Shear-layer flow regimes and wave instabilities and reattachment lengths downstream of an abrupt circular channel expansion, *J. Appl. Mech.* **39**, 677–681 (1972).
3. A. Pollard, A contribution on the effects of inlet conditions when modelling stenoses using sudden expansions, *J. Biomechanics* **14**, 349–355 (1981).
4. D. J. Latornell and A. Pollard, Some observations on the evolution of shear layer instabilities in laminar flow through axisymmetric sudden expansions, *Phys. Fluids* **29**, 2828–2835 (1986).
5. A. J. Ede, C. I. Hislop and R. Morris, Effect on the local heat-transfer coefficient in a pipe of an abrupt disturbance of the fluid flow: abrupt convergence and divergence of diameter ratio 2/1, *Proc. Inst. Mech. Engrs* **170**, 1113–1126 (1956).
6. M. Prud'homme and S. Elghobashi, Turbulent heat transfer near the reattachment of flow downstream of a sudden pipe expansion, *Numer. Heat Transfer* **10**, 349–368 (1986).
7. J. W. Baughn, M. A. Hoffman, B. E. Launder, D. Lee and C. Yap, Heat transfer, temperature, and velocity measurements downstream of an abrupt expansion in a circular tube at a uniform wall temperature, *ASME J. Heat Transfer* **111**, 870–876 (1989).
8. D. F. Fletcher, S. J. Maskell and M. A. Patrick, Heat and mass transfer computations for laminar flow in an axisymmetric sudden expansion, *Computers Fluids* **13**, 207–221 (1985).
9. C. G. Caro, J. M. Fitz-Gerald and R. C. Schroter, Atheroma and arterial wall shear observation, correlation and proposal of a shear dependent mass transfer mechanism for atherogenesis, *Proc. Roy. Soc. Lond.* Series B, **177**, 109–159 (1971).
10. C. K. Zarins, D. P. Giddens, B. K. Bharadvaj, V. S. Sottiurai, R. F. Mabon and S. Glagov, Carotid bifurcation atherosclerosis: quantitative correlation of plaque localization with flow velocity profiles and wall shear stress, *Circ. Res.* **53**, 502–514 (1983).
11. D. N. Ku, D. P. Giddens, C. K. Zarins and S. Glagov, Pulsatile flow and atherosclerosis in the human carotid bifurcation: positive correlation between plaque localization and low and oscillating shear stress, *Arteriosclerosis* **5**, 293–302 (1985).
12. E. J. Watson, Diffusion in oscillatory pipe flow, *J. Fluid Mech.* **133**, 233–244 (1983).
13. C. H. Joshi, R. D. Kamm, J. M. Drazen and A. S. Slutsky, An experimental study of gas exchange in laminar oscillatory flow, *J. Fluid Mech.* **133**, 245–254 (1983).
14. U. H. Kurzweg, Temporal and spatial distribution of heat flux in oscillating flow subjected to an axial temperature gradient, *Int. J. Heat Mass Transfer* **29**, 1969–1977 (1986).
15. R. A. Peattie, Heat transfer in laminar, oscillatory flow in cylindrical and conical tubes, *Int. J. Heat Mass Transfer* **32**, 923–934 (1989).

16. M. F. Hwang and A. Dybbs, Heat transfer in a tube with oscillatory flow, *ASME Paper* 83-*WA/HT*-90, pp. 1–12 (1983).
17. R. Siegel, Influence of oscillation-induced diffusion on heat transfer in a uniformly heated channel, *ASME J. Heat Transfer* **109,** 244–247 (1987).
18. V. V. Mamayev, V. S. Nosov and N. I. Syromyatnikov, Investigation of heat transfer in pulsed flow of air in pipes, *Heat Transfer—Sov. Res.* **8,** 111–116 (1976).
19. J. S. Park, M. F. Taylor and D. M. McEligot, Convective heat transfer for ship propulsion, *7th Annual Summary Report*, University of Arizona, Tucson, AZ (1982).
20. S. K. Gupta, R. D. Patel and R. C. AcRerverg, Wall heat/mass transfer in pulsatile flow, *Chem. Engng Sci.* **37,** 1727–1739 (1982).
21. H. W. Cho and J. M. Hyun, Numerical solutions of pulsating flow and heat transfer characteristics in a pipe, *Int. J. Heat Fluid Flow* **11,** 321–330 (1990).
22. A. A. Al-Haddad and N. Al-Binally, Prediction of heat transfer coefficient in pulsating flow, *Int. J. Heat Fluid Flow* **10,** 131–133 (1989).
23. W. J. McMichael and J. D. Hellums, Interphase mass and heat transfer in pulsatile flow, *A.I.Ch.E. Jl* **21,** 743–752 (1975).
24. Fluent Inc., *FLUENT User's Manual*, Version 3.03. Lebanon, NH (1991).
25. S. V. Patankar, *Numerical Heat Transfer Fluid Flow*, Hemisphere Publishing Corp., Washington, DC (1980).
26. P. Ma, The role of fluid flow and mass transfer on atherosclerosis in the human carotid bifurcation, PhD Thesis, Georgia Institute of Technology, Atlanta (1992).
27. J. R. Womersley, Method for the calculation of velocity, rate of flow and viscous drag in arteries when the pressure gradient is known, *J. Physiol.* **127,** 553–563 (1955).
28. Dow Corning Co., *Information about Thermometric Fluids*. Dow Corning, Midland, MI (1990).
29. R. K. Shah and M. S. Bhatti, Laminar convective heat transfer in ducts. In *Handbook of Single-Phase Convective Heat Transfer* (Edited by S. Kakac, R. K. Shah and W. Aung), Chap. 3. John Wiley and Sons, New York (1987).
30. V. K. Garg and S. Jayaraj, Boundary layer analysis for two-dimensional slot jet impingement on inclined plates, *ASME J. Heat Transfer* **110,** 577–582 (1988).
31. R. J. Goldstein and M. E. Franchett, Heat transfer from a flat surface to an oblique impinging jet, *ASME J. Heat Transfer* **110,** 84–90 (1988).
32. E. M. Sparrow and B. J. Lovell, Heat transfer characteristics of an obliquely impinging circular jet, *ASME J. Heat Transfer* **102,** 202–209 (1980).
33. M. Kurosaka, J. B. Gertz, J. E. Graham, J. R. Goodman, P. Sundaram, W. C. Riner, H. Kuroda and W. L. Hankey, Energy separation in a vortex street, *J. Fluid Mech.* **178,** 1–29 (1987).
34. X. He and D. N. Ku, Unsteady entrance flow development in a straight tube, *J. Biomech. Engng*, in press.